"Galileo Galilei-GG"
Answers to Questions as formulated by ESA M4 "Science Assessment Review Panel-SARP"

Anna M. Nobili, on behalf of the GG Team
(Dated: 15 April 2015)

We find it appropriate to start by answering Q2 because in so doing we can eliminate a quite common misunderstanding on the rotation of GG and help the rest of the discussion.

II. Since no explicit mention is made of the elastodynamic constitutive properties of either cylinder they appear to be treated as perfectly rigid.

Q2. What is the possibility that a small time dependent axial, lateral or torsional deformation of the cylinders (e.g. transmitted by bearings reactions to tidal forces or torques) could induce a differential motion between the cylinders that could mimic a signal arising from any differential couplings of terrestrial gravity to them?

A2. The question Q2 hints at possible disturbing effects on the test masses due to the bearings.

Sec. 1.4 of the GG proposal is devoted to how crucial is to perform the GG experiment in space (*Sec. 1.4 The role of space in testing UFF/WEP: is it crucial or is it an option? pp. 14-15*). On p. 15 it reads *"Finally, being isolated in space the whole spacecraft can spin (as torsion balances do) needing no motor and no bearings (passive one axis stabilization), simply by angular momentum conservation."*

While on the ground any rotating object has a rotating and a non-rotating part (rotor and stator), and therefore needs bearings between the two (GGG has ceramic ball bearings; see answer A7 below for bearings noise), the 1 Hz rotation of GG is provided at the start of the mission and needs neither motor nor bearings. The entire spacecraft, made of the outer shell, the PGB intermediate stage and the test cylinders, all arranged as a Russian doll, is co-rotating. It is similar to the diurnal rotation of the Earth and its atmosphere, which obviously has neither motor nor bearings. At ESTEC, (52° latitude) the linear velocity relative to inertial space is about 1000 km/hr. On the outer surface of GG it is 11 km/hr.

In GG, should a small differential rotation arise between the outer shell and the PGB (because of temperature effects), it will be detected by a simple optical system and corrected by cold gas thrusters; the issue was studied in great detail for an equatorial orbit, in which case the effect is relevant because of large temperature effects at the orbital frequency induced by the satellite being about half of its orbital period in sunlight and half in the Earth's shadow (see [1], Sec. 2.1.2).

In principle tidal effects from the Earth on each test cylinder may cause deformations. It is known that celestial bodies can be torn apart by tidal forces, but we can show that this effect is totally negligible in GG. For the larger test mass (Be; 10 kg, 10.5 cm internal radius, 13 cm external radius, 28.6 cm height) the tidal differential acceleration from Earth in the sensitive plane (perpendicular to the spin/symmetry axis) is:

$$\Delta a_{Tide\oplus} \simeq \frac{3GM_\oplus}{d_{orb}^3}\Delta \simeq 3.5\cdot 10^{-6}\cdot 0.25 \simeq 8.7\cdot 10^{-7}\,\mathrm{m/s^2} \quad (1)$$

at an orbiting distance $d_{orb} \simeq 7\cdot 10^6$ m and for a maximum separation distance $\Delta\simeq$25 cm between two half-cylinders of 5 kg each. The corresponding differential force is $\simeq 5\cdot 8.7\cdot 10^{-7} \simeq 4.3\cdot 10^{-6}$ N exerting a pressure $\simeq 4.3\cdot 10^{-6}/(0.025\cdot 0.28\cdot 2) \simeq 3\cdot 10^{-4}$ Pa. This pressure must be compared with the Young's modulus, which measure the stiffness of the material, and for Be is a few hundreds of GPa, about 15 orders of magnitude larger. The Young's modulus of Ti is a few times smaller, but the Ti cylinder is smaller in size, hence the result is about the same.

Even in the event of using test masses made of Polyethylene and Lead (for the reasons reported in the Executive Summary) possible deformations due to Earth tides would be negligible by orders of magnitude.

Q3. Furthermore it is known that in some circumstances whirling motions can become chaotic. Could such motions in the experiment be initiated and how would they then be eliminated in space? Please provide details of how such motions are modelled in the simulator.

A3. The assumption that GG has rotor, stator and bearings like ground-based rotors may have led to worry that its motion may become chaotic. For such rotors the literature on rotordynamics reports cases of chaotic motion: *Chaotic Behavior of Rotor/Stator Systems With Rubs* [2], *Instability of Unbalance Excited Synchronous Forward Whirl at Rotor-Stator-Contact* [3], *Chaotic motions of a rigid rotor in short journal bearings* [4]. GG has nothing to do with them. In addition, it has very small internal damping (contrary to supercritical rotors of practical use).

The basic equations of motion for a 2D mechanical oscillator in supercritical rotation and very low internal damping have been published in compact form in a Letter to Physical Review [5]. While the equations of the

complete system used in the GG simulator are given, as requested, in response to Q4 (see Appendix on the GG simulator), it is worth to report here their main features as outlined in [5].

In essence, the GG concentric test cylinders form a 2D harmonic oscillator as shown in Fig. 1

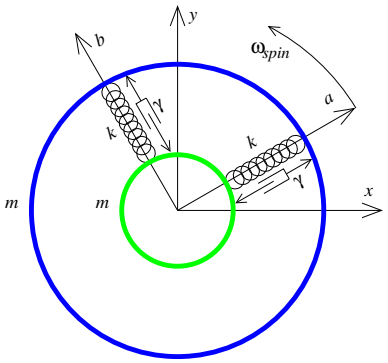

FIG. 1: Sketch of the 2D rotating oscillator. The proof masses are concentric and rotate –together with the springs– at angular velocity ω_{spin}. They are assumed for the moment as perfectly centered on the rotation axis. The springs are modeled as ideal springs of elastic constant k and zero length at rest; to each spring is associated a co-rotating thermal noise force generator F_{th} and an ideal noiseless damper γ. x, y is the inertial frame; a, b is the rotating one.

Let us now write and solve the equations of motion of the 2D rotating oscillator around the equilibrium position in the presence of a l force, like the signal, of very low frequency. Once the system has been reduced to a single body of reduced mass $\mu = m/2$ and natural frequency $\omega_n = \sqrt{k/(m/2)}$ the equations of motion in the inertial frame read:

$$\mu\ddot{\vec{r}} + \gamma_{\omega_{spin}}(\dot{\vec{r}} - \vec{\omega}_{spin} \times \vec{r}) + k\vec{r} = \vec{F} \tag{2}$$

$\gamma_{\omega_{spin}}$ is the small internal damping $\gamma(\omega) \simeq \frac{k\phi(\omega)}{\omega}$ of the oscillator with elastic constant k and loss angle ϕ rotating at ω_{spin}; $\vec{F}$ is the signal force whose frequency is so small compared to both ω_{spin} and ω_n that we assume a constant force for simplicity. In the assumptions made ($\omega_{spin} \gg \omega_n$ and very small internal losses) the solution of the homogeneous part of (2) is:

$$\begin{aligned}\vec{r}_w(t) \simeq A_0 e^{\phi_{\omega_{spin}}\omega_n t/2}\begin{pmatrix}\cos(\omega_n t + \varphi_A)\\ \sin(\omega_n t + \varphi_A)\end{pmatrix} + \\ + B_0 e^{-\phi_{\omega_{spin}}\omega_n t/2}\begin{pmatrix}\cos(-\omega_n t + \varphi_B)\\ \sin(-\omega_n t + \varphi_B)\end{pmatrix}\end{aligned} \tag{3}$$

(with amplitudes and phases determined by initial conditions), showing that in the inertial reference frame the oscillator performs a combination of a forward and a backward orbital motion –known as *whirl motion*– at the (slow) natural frequency ω_n, and the radii of such orbits are exponentially decaying in the case of the backward whirl and exponentially growing in the case of the forward one. We have written the exponential behavior in terms of the small loss angle:

$$\phi_{\omega_{spin}} \simeq \frac{\gamma_{\omega_{spin}}\omega_{spin}}{\mu\omega_n^2} = \frac{\gamma_{\omega_{spin}}\omega_{spin}}{k} \tag{4}$$

The forward whirl is then a very weak instability. Every natural/whirl period the radius of the forward whirl grows by the fraction $\pi\phi_{\omega_{spin}}$, hence the tangential force which produces the growth is –in modulus– $\phi_{\omega_{spin}} kr$, which is a very small fraction of the elastic force, requiring a correspondingly small force to stabilize it. Its frequency is the natural one and does not interfere with the signal (see [6], [8]).

In the presence of an external constant force $\vec{F}$, the equations of motion (2) show that (in the inertial frame) the body is displaced to the position:

$$\begin{aligned}\vec{r}_F(t) = \frac{1}{1 + \frac{\gamma^2_{\omega_{spin}}\omega^2_{spin}}{k^2}} \\ \cdot\left(\frac{\vec{F}_e}{k} - \frac{\gamma_{\omega_{spin}}}{k^2}\vec{\omega}_{spin} \times \vec{F}\right) \simeq \frac{\vec{F}}{k} - \phi_{\omega_{spin}}\frac{\vec{\omega}_{spin}}{\omega_{spin}} \times \frac{\vec{F}}{k}\end{aligned} \tag{5}$$

As we can see, the applied force $\vec{F}$ gives rise to a displacement $\vec{F}/k$ (i.e. the displacement is inversely proportional to the natural frequency squared) and unaffected by rotation, with an additional effect in the orthogonal direction due to rotation which is negligible because of the very small loss angle $\phi_{\omega_{spin}}$. In the rotating frame of the oscillator this constant displacement observed in the inertial one appears at the rotation frequency $\omega_{spin} \gg \omega_n$, yet it is apparent that no attenuation occurs. Instead, it is well known that for an oscillator with 1 degree of freedom, the displacement due to a force at frequency $\omega_{spin} \gg \omega_n$ drops off as $(\omega_n/\omega_{spin})^2$. Note that the signal-to-thermal noise ratio is the same in the two cases, since the displacement due to the signal and that due to the thermal noise force are either both unchanged (by the 2D oscillator) or both attenuated (by the 1D oscillator). When dealing with extremely weak effects a signal whose strength is not attenuated by rotation has the advantage to loosen the requirements on the performance of the read out, as long as rapid rotation takes care of up-converting the signal to a frequency at which thermal noise is much lower.

The general solution of the 2D rotating oscillator in the inertial frame is:

$$\begin{aligned}\vec{r}(t) \simeq -\vec{\epsilon}(\omega_{spin}t)\left(\frac{\omega_n}{\omega_{spin}}\right)^2 + \frac{\vec{F}}{k} - \phi_{\omega_{spin}}\frac{\vec{\omega}_{spin}}{\omega_{spin}} \times \frac{\vec{F}}{k} + \\ + A_0 e^{\phi_{\omega_{spin}}\omega_n t/2}\begin{pmatrix}\cos(\omega_n t + \varphi_A)\\ \sin(\omega_n t + \varphi_A)\end{pmatrix} + \\ + B_0 e^{-\phi_{\omega_s}\omega_n t/2}\begin{pmatrix}\cos(-\omega_n t + \varphi_B)\\ \sin(-\omega_n t + \varphi_B)\end{pmatrix}\end{aligned} \tag{6}$$

which is helpful to comment as follows. Assume zero losses and no external force: only the first term is not zero and the solution is the auto-centered position rotating at frequency ω_{spin}; if the force signal $\vec{F}$ is added –still with zero losses– the term $\vec{F}/k$ is not zero and the oscillator is displaced by this vector with auto-centering holding as before; finally, if small losses occur –after the backward whirl has died out, and neglecting the small effect $\propto \phi_{\omega_{spin}}$– the forward whirl slowly grows around the displaced position at frequency ω_n. By controlling this weak instability, rotation (and signal modulation) at a frequency much higher than the natural one are achieved with thermal noise is much lower and the signal is not attenuated (see [5]).

There is no question that having 2 degrees of freedom –as sketched in Fig. 1– instead of being constrained in 1 direction (while rotating perpendicular to it), is the key dynamical feature of the oscillator which makes fast rotation physically possible, thus ensuring up-conversion of the signal to much higher frequency where the competing thermal noise due to internal losses is much smaller.

Indeed, this is the key feature of GG, by which it can aim at 10^{-17}-10^{-18} like STEP while being small and at room temperature like Microscope.

It is worth recalling that the whirl motion issue has been the subject of many discussions, well documented in the literature.

In 1997 it was the subject of a discussion which involved S. H. Crandall, a highly reputed MIT expert in rotordynamics, who strongly supported the point of view of the GG group (see [7–9]). Since then, in GGG, whirl motions have been routinely stabilized by tiny forces fully in accord with those early estimations. An experimental result which confirms an important theoretical prediction on whirl damping has been obtained recently (not yet published) and it is reported below in response to Q7.

I. The breakdown of the WEP is sought in the framework of the response of test matter to terrestrial Newtonian gravitation. The source of terrestrial Newtonian gravitation is independent of the earth's (non-uniform) rotation while in general relativity the gravitational filed of a rotating source depends on its angular momentum. Furthermore, the test cylinders in the proposed experiment are rotating and the motion of extended spinning test matter in an esternal gravitational filed may depend on its rotation rate

Q1. Based on general relativity what are the expected effects of the earth's rotation and cylinder rotation on the motion of each spinning cylinder and their relevance to the interpretation of any non-null signal?

A1. In General Relativity (GR) the effect of the rotation of a primary mass (the Earth in our case) is manifested in its gravitomagnetic field. Outside the mass, in the simplified assumption that the Earth is rigid, axially symmetric in space and its angular velocity is constant, the gravitomagnetic field has a dipolar structure which is directly related to the Earth's angular momentum $\mathbf{J}_\oplus$. This is intrinsic gravitomagnetism produced by mass-currents and it generates additional space-time curvature [10]. From the point of view of the space-time metric $g_{\mu\nu}$ such effects are described by the off-diagonal components of the Kerr metric [11]:

$$ds^2 = \left(1-\frac{2GM_\oplus}{rc^2}\right)c^2dt^2 - \left(1+\frac{2GM_\oplus}{rc^2}\right)dr^2 - r^2d\theta^2 - r^2\sin^2\theta d\varphi^2 + \frac{4GJ_\oplus}{rc^2}\sin^2\theta d\varphi dt, \tag{7}$$

which is an exact solution of Einstein's field equations. In the above equation, t is the *coordinate time*, r is the radial coordinate, θ and φ are the spherical coordinates.

The Kerr metric as written above is valid in the weak-field and slow motion (WFSM) limit of GR, i.e. $\frac{GM_\oplus}{rc^2} \ll 1$ and $\frac{J_\oplus}{M_\oplus rc} \ll 1$. It describes the metric generated by a central body (the primary) with mass $M_\oplus$ and angular momentum (intrinsic spin) $\mathbf{J}_\oplus$.

The effect of the gravitational field on a freely falling gyroscope (e.g a spinning hollow cylinder as in GG) is a precession of its axis. The effect is due to both the Newtonian part of the field –leading to the *geodetic precession* around a direction perpendicular to the orbit plane– and to the gravitomagnetic part –producing a *frame dragging* that manifests itself as a precession around the lines of force of the terrestrial gravitomagnetic dipole.

Therefore, as a consequence of the Earth's rotation there is an effect (known as *frame dragging*) in addition to the effect which is present in the case of a static background –as that described by Schwarzschild metric– i.e. the *geodetic precession* While the latter does not depend on the angular momentum of the Earth, neither on that of the cylinder, the precession due to frame dragging is proportional to the angular momentum $\mathbf{J}_\oplus$ of the Earth.

It is worth mentioning that while the gravitomagnetic precession can be considered as a *spin-spin* interaction, the geodetic precession may be considered as a *spin-orbit* interaction (see [12]):

Their mathematical expressions are:

$$\mathbf{\Omega}_{\mathrm{geo}\oplus} = \frac{3}{2}\frac{GM_\oplus}{c^2r^3}\mathbf{r}\times\mathbf{v}, \tag{8}$$

for the Earth's geodetic precession ($\mathbf{r}$ and $\mathbf{v}$ are the istantaneous position and velocity of the gyroscope with respect to the Earth), and

$$\mathbf{\Omega}_{\mathrm{grav}} = \frac{G}{c^2r^3}\Big(3\hat{\mathbf{r}}(\hat{\mathbf{r}}\cdot\mathbf{J}_\oplus) - \mathbf{J}_\oplus\Big), \tag{9}$$

for the Earth's gravitomagnetic precession.

For an Earth orbiting gyroscope (8) and (9) are the most relevant precessions. There is also an additional one, due to the motion of the Earth in the static-field of the Sun, which reads:

$$\mathbf{\Omega}_{\mathrm{geo}\odot} = \frac{3}{2}\frac{GM_\odot}{c^2R^3}\mathbf{R}\times\mathbf{V}, \tag{10}$$

where $\mathbf{R}$ and $\mathbf{V}$ are the position and velocity of the Earth with respect to the Sun. It is mathematically identical to the terrestrial precession, but it is obviously the same for all gyroscopes regardless of their orbit around the Earth. Precession occurs around the normal to the ecliptic plane.

It may be helpful to recall that the geodetic precession is also known as de Sitter precession [13]. The gravitomagnetic precession of a gyroscope is also known as the Schiff frame-dragging effect [14], similar (but not identical) to the frame-dragging effect of the orbital plane, also known as Lense-Thirring effect [15].

These precessions do not affect the center of mass of the gyroscopes because within GR they must obey WEP (a rotating and a non rotating body must fall with the same acceleration in any external gravitational field).

For the numerical values of the three precessions we obtain:

$$\Omega_{\mathrm{geo}\oplus} \sim \frac{c}{r}\left(\frac{GM_\oplus}{c^2r}\right)^{\frac{3}{2}} \sim 10^{-12}\ \mathrm{rad/s}, \tag{11}$$

$$\Omega_{\mathrm{grav}} \sim \frac{GJ_\oplus}{c^2r^3} \sim 10^{-14}\ \mathrm{rad/s}, \tag{12}$$

$$\Omega_{\mathrm{geo}\odot} \sim \frac{c}{R}\left(\frac{GM_\odot}{c^2R}\right)^{\frac{3}{2}} \sim 10^{-15}\ \mathrm{rad/s}. \tag{13}$$

The rule of thumb estimates assume $r \simeq 7000$ km for the orbital radius of GG.

The geodetic and frame dragging precessions have been measured by the (almost perfect) gyroscopes of GPB [16] for a polar, almost circular ($e <\simeq 0.0014$) orbit at 642 km altitude. Their values are 6.6 as/yr and 39 mas/y respectively. The orbit of GG is similar to that of GPB (98°

inclination, 630 km orbit, small eccentrcity) and we can therefore use the same values. Indeed, if we integrate over a year the values estimated in (11) and (12), we obtain values very close to those measured by GPB.

Any differential precession must involve an offset ε between the centres of mass of the test cylinders and is therefore reduced by the factor ε/r, which in GG is extremely small.

The solar geodetic precession amounts to about 19 mas/yr (and is the same for all gyroscopes).

Let us know consider the differential linear accelerations. In GR, the angular momentum of the Earth affects the free fall of a *non-spinning* test mass through the geodetic equations:

$$\frac{d^2x^\alpha}{d\tau^2} + \Gamma^\alpha_{\beta\gamma}\frac{dx^\beta}{d\tau}\frac{dx^\gamma}{d\tau} = 0, \tag{14}$$

where $\Gamma^\alpha_{\beta\gamma}$ are the Christoffel symbols and τ the proper time measured by a hypothetical clock comoving with the gyroscope, i.e. our test "particle".

In the case of the geodetic precession, which is responsible for the largest variation in the direction of the axis of rotation of the GG test cylinders, for the radial "gravitational acceleration" we obtain:

$$a^r = \frac{d^2r}{d\tau^2} = -\Gamma^r_{00}\left(\frac{dt}{d\tau}\right)^2 - 2\Gamma^r_{0i}\frac{dt}{d\tau}\frac{dx^i}{d\tau} - \Gamma^r_{ij}\frac{dx^i}{d\tau}\frac{dx^j}{d\tau}. \tag{15}$$

The lowest order expression (in $J_\oplus/r^2$) of the Christoffel $\Gamma^r_{0\phi}$ is:

$$\Gamma^r_{0\phi} \simeq -G\frac{J_\oplus}{c^2r^2}\sin^2\theta. \tag{16}$$

Consequently the correction to the radial acceleration (again assuming a Keplerian orbit) is (see also Ref. [17]):

$$a^r_{\mathrm{geo}\oplus} \sim \frac{GJ_\oplus}{c^2r^3}v, \tag{17}$$

and for its numerical value we obtain:

$$a^r_{\mathrm{geo}\oplus} \sim 9.5\cdot 10^{-11}\ \mathrm{m/s^2}. \tag{18}$$

For the corresponding fractional differential acceleration we obtain:

$$\frac{\Delta a}{g(h)} \simeq 3\frac{\varepsilon}{r}\frac{a^r_{\mathrm{geo}\oplus}}{g(h)} \approx 5\cdot 10^{-18}\varepsilon, \tag{19}$$

where $g(h)\simeq$8.1 m/s^2 is the Earth's driving acceleration at the spacecraft altitude h.

By construction, the offset between the GG test masses is required to be 10 μm. After self-centering in supercritical rotation the largest remaining separation between the test masses is due to whirl motion (at the natural differential period of 540 s) and is required not to exceed 10^{-9} m (see GG proposal, Sec. 2.2.3 Driver #3: Centers of mass centering, Table 6, p. 20).

This gives:

$$\frac{\Delta a}{g(h)} \approx 5\cdot 10^{-27}, \tag{20}$$

which is almost 10 orders of magnitude smaller than the GG baseline target.

Terms quadratic in the velocities are even smaller. The spin-spin attractive-repulsive interaction is higher order, then negligible. Any differential effect is multiplied by $\varepsilon/r \sim 10^{-16}$, hence totally negligible.

In conclusion, all the analyzed effects are negligible and need not to be taken into account in GG.

III. The error budget in section 3.3 is critical for the expected accuracy claimed for the experiment. The figures appear to be based on GGG tests and an end-to-end simulator. In particular the proposal refers to a "WEP Inertial Frame" that does not spin. However, it is difficult to ascertain from section 3.2.1 precise details of the modelling assumption behind many of the simulation results

Q4. Please provide more information on these details and explain how the results in columns 2 and 4 in Table 12 and those in Table 8 are obtained? In particular provide the differential equations for the model used to ascertain the motion of each (spinning) cylinder in the earth's gravitational field?

A4. The page limit on M4 proposals has not allowed us to include much details on the error budget and the simulator, which have been the subject of intensive work over many years and in particular during the 2008-2009 industrial study by Thales Alenia Space Italy (funded by the Italian Space Agency). which resulted in more than 30 documents [18]. A summary report on the GG simulator, the equations of motion and the results is attached in an Appendix at the end of this document.

Here we provide answers on the "WEP Inertial Frame", on Table 12 and on Table 8.

The sought for violation signal is a differential displacement vector between the centres mass of the test cylinders (which form the GG accelerometer) pointing to the center of mass of the Earth as the GG satellite orbits around it (see Fig. 1 of the GG Proposal), hence it is at the orbital frequency $\nu_{orb} \simeq 1.7 \cdot 10^{-4}$ Hz.

The natural frequency of oscillation of the test cylinders in differential mode (540 s natural differential period) translates the differential displacement into a differential acceleration. If a differential acceleration is measured, with the known signature of a violation signal and different from all known systematics, its ratio to the acceleration from Earth ($g(h) \simeq 8.1\,\mathrm{m/s^2}$ at the orbiting altitude $h \simeq 630$ km) yields the Eötvös parameter η; the goal of GG as baseline mission being $\eta = 10^{-17}$.

In the sensitive plane of the accelerometer (perpendicular to the spin/symmetry axis of the test cylinders) the signal is up-converted from the orbital to the spin frequency, a fact which has well known advantages. Given that all original data taken in the spinning frame are available, it is convenient to demodulate back to a non-spinning frame in which the signal is at the orbital frequency and disturbances whose frequency is, say, twice or three times the orbital frequency appear well separated from it (while in the spinning frame they are all very close to $\nu_{spin} = 1$ Hz since they differ from it by about 10^{-4} Hz only). This is only a matter of convenience, allowing us to produce a very compact synoptic plot (as shown in Fig. 12 of the GG proposal) which is a graphical, effective way of presenting the error budget (see below the discussion on Table 12 and Fig. 12).

This is how the "WEP Inertial Frame" comes into play. It is defined as follows. It is centered on the center of mass of one test cylinder (TM1). The z axis is aligned with the spin axis, which has the useful property of being essentially fixed in inertial space because the high spin energy of GG (at 1 Hz spin rate) makes it insensitive to external torques. The x axis is aligned with the X axis of the inertial J2000 reference frame (from the Earth to the γ point at the date 01/01/2000) and the y axis completes the system, which does not spin. The x, y plane, being perpendicular to the spin axis but non spinning, contains the signal after demodulation, i.e. at the orbital frequency. Note that the spin frequency is defined relative to the fixed stars, not relative to the Earth (they differ from one another by the orbital frequency). An observer in this frame, sitting on TM1, sees the Earth orbiting around it at frequency ν_{orb} (with the appropriate sign); in case of violation he measures a displacement vector of TM2 from the origin, always pointing to the Earth, hence also at orbital frequency. It is apparent that this reference frame is inertial.

In the lab the GGG accelerometer is suspended against local gravity along the spin/symmetry axis of the cylinders, thus the analog of the x, y plane is the horizontal plane of the lab.

We can now look at the error budget table of the GG proposal (Table 12). Columns 2 gives the frequency at which each listed effect appears in the "WEP Inertial Frame" defined above. Column 4 gives the value of the differential acceleration Δa that each effect produces between the test cylinders (at the corresponding frequency).

The first entry is the target violation signal of the GG baseline mission (η=10^{-17}), whose frequency is the orbital one and whose magnitude is $\Delta a = g(h)\eta = 8.1 \cdot 10^{-17}\,\mathrm{m/s^2}$. The following entries list perturbations (systematic errors) whose frequency is either ν_{orb} like the signal or close to it; the closer is the frequency of a perturbation to ν_{orb}, the most carefully it must be dealt with in order to separate it from the signal. Systematic errors can be discriminated from the signal if their specific signature (different from the known signature of the signal) is known and a large enough number of measurements is performed in different dynamical conditions so that such differences can become apparent. In GG this is possible thanks to the low thermal noise [5] and consequent short integration time [19] whereby one full measurement to the target sensitivity can be performed in one day only. While the spin axis of GG is fixed in inertial space, its orbit plane undergoes a nodal regression of about 1°/d, thus providing the required change of dynamical conditions which allows the signature of each effect to show up.

Table 12 and Fig.12 encompass the result of a 90 d measurement cycle, and the GG simulator (see Appendix) allows us to firmly establish the frequency and size of the various systematic errors. The most important result to be stressed concerns the coupling of the Earth's

monopole with the (different) quadruple mass moments of the test cylinders. While in a single measurement covering many days it is undistinguishable from a violation signal (it is at ν_{orb} and points to the Earth, just like the signal) it is easy to show (analytically) that in a day by day evolution this effect has an additional component at $3\,\nu_{orb}$. Similarly, tidal effects which in a single measurement have only twice the orbital frequency, in a day by day evolution have also an effect at 4 times the orbital frequency. The dynamical evolution of GG in sun synchronous orbit and the ability to make one measurement per day allow us to firmly discriminate these effects from the signal.

Note that in Fig.12 all effects (each at its own frequency and with its own color code) are expressed as differential displacements of the test cylinders, while in Table 12, column 4 we list (for the most relevant effects) the corresponding differential acceleration (in m/s^2). The two are consistent. They are simply related as $\Delta r \simeq \frac{\Delta a}{4\pi^2} \cdot P_{dm}^2$ with $P_{dm} = 540\,\mathrm{s}$ the period of natural oscillation of the test cylinders in differential mode. For a violation signal at $\eta = 10^{-17}$ and $\Delta a_{_{WEP}} = 8.1 \cdot 10^{-17}\,\mathrm{m/s^2}$ we have $\Delta r_{_{WEP}} \simeq \frac{\Delta a_{_{WEP}}}{4\pi^2} \cdot P_{dm}^2 \simeq 0.6 \cdot 10^{-12}\,\mathrm{m}$.

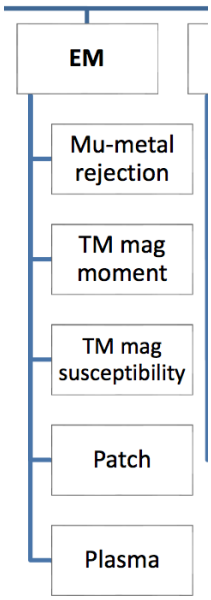

FIG. 2: The electromagnetic driver (taken from Fig. 2, p. 17 of the GG proposal) with blocks showing all issues which need to be taken care of (by meeting specific requirements) in order to make the corresponding effects not dangerous.

Concerning the question on Table 8, please note that we use the concept of experiment drivers, of which a global view is shown in Fig. 2, p. 17. For each experiment driver the corresponding Table in Sec. 2.2 reports, in a very compact form, the key data and the corresponding requirements. Data and requirements often result from a considerable amount of work which could not possibly be incorporated in the GG proposal, hence they may not be easy to follow by the reviewer.

Table 8 refers to "Driver # 5: Electromagnetic disturbances". As shown in Fig.2 the electromagnetic "driver" requires to deal with: μ-metal shielding (to reduce the Earth's magnetic field); the residual magnetic moment and magnetic susceptibility of the test bodies; the electric patch effect and the residual plasma effect. Table 8 reports the conclusion of our investigation; some details have been reported in [18], some are the subject of internal notes.

Reviewers may not be familiar with the effect of residual plasma, of which we have not been aware until it was pointed out by F. Pegoraro during the 2009 industrial study. In GG we do not fly a vacuum chamber, but obtain vacuum for free by venting to outer space. However, care must be taken when opening a connection hole between the spacecraft and outer space. Even at low Earth orbit as in the case of GG some plasma already exists which gives rise to a current on the satellite surface, which in turn, because of the Earth's magnetic field, will produce a (non gravitational) force on it which in turn will be felt as an equal and opposite inertial force (in common mode) by all bodies suspended inside the spacecraft. It has been demonstrated [20] that at typical GG altitudes such a force –even under extremely conservative assumptions– is below 1/1000 of the typical residual air (neutral) drag force, and therefore poses no problems to the drag free control system of GG. However, this is correct as long as the outside plasma is not allowed inside the spacecraft. A non gravitational acceleration 1000 times smaller than drag, acting directly on the PGB and the test masses, would leave a residual differential effect larger than the signal. This would likely happen because some plasma might get inside the spacecraft through the openings mentioned above. A cure for that has already been found and successfully implemented in the BeppoSax mission to protect its sensors. It is based on two appropriate grids for each opening (one neutral and one charged) so as to keep the plasma out and it has been adapted to the case of GG [20].

A more widely known issue is that of residual electric patches, which are expected even for electrically grounded test masses as in GG (only their time variations at the low orbital frequency are relevant). In addition to known mitigations (such as coating), in GG we significantly reduce this effect by having large gaps between the test masses (2.5, cm), which is made possibile by using the laser gauge instead of the capacitance readout (300 μm in GOCE, 600 μmin Microscope, a few mm in LISA-PF).

In addition, we have devised and tested in GGG a simple method for measuring the direct mechanical effect of patches using capacitance plates and exploiting the simple fact that when the sign of an applied potential is changed, the sign of the applied charge changes too, while the sign of the patch charge does not. In this

way, by applying unipolar and bipolar square wave potential at a given frequency it is possible to produce a signal which depends on the patch charge in an unambiguous way. We have performed the test on GGG (while spinning) for 10.6 days, in order to measure the low frequency time variations of the patch amplitude (which would indicate a variation of the patch charge). We used a small capacitance plate ($4\,\mathrm{cm}^2$) and had no gold coating, while smaller patch charges are expected for larger surfaces with gold coating. Thus, we were in worst case conditions. At diurnal frequency we measured several micro Volt. The method can in principle be used also in the space experiment, though lab tests can rule out the danger of patches in GG.

Finally, Table 8 reports the effects due to the magnetic field of the Earth for the case of GG in sun synchronous, quasi-polar orbit at about 630 km altitude (past publications report these effects for the case of GG in equatorial orbit). The largest of such effects (at twice the orbital frequency) is due to the interaction between the residual dipole moment of one test mass with the magnetic moment induced on the other by the Earth's magnetic field. It is well below the signal if a μ-metal shield is applied (on the PGB) to attenuate the Earth's field by a factor 150. This is not a demanding shielding, and it could be improved should measurements of the actual test cylinders give values of the residual magnetic moments and the magnetic susceptibility higher than expected.

Please refer to the Appendix for the GG end-to-end simulator, the equations of motion and how the error budget is constructed, in both tabular and graphical form.

IV. The laser gauge readout plays a critical role in achieving the predicted performance. Please clarify the overall design of the laser gauge device and state clearly how it will be made fully operational in time for a possible flight and indicate the role that the gauge plays in the final target sensitivity.

The laser gauge described in the proposal is based on standard technologies and fully proven principles. The peculiarity of the device is in its compactness and in the layout of the components. Most of the components are off-the-shelf and only a few custom coatings are needed. The plan for its realization is based on a phase of design and optical simulation which will lead to the sizing of the prototype (in particular the size and the shape of the masks discussed below). The prototype will be built and tested in vacuum stimulated with displacement signals (at the scale of the science signals) in order to test noise, cross-talk, and thermal stability. We confirm the statement made in the proposal that in one year we can bring it to TRL 5.

Q5. In particular:

a) What is the effect of satellite acceleration on the predicted performance of the laser gauge measurement system?

The largest non gravitational acceleration acting on the outer shell of the GG spacecraft is due to residual air along the orbit at about 630 km altitude, the largest component being at the orbital frequency (up-converted to the spin frequency). This component will be reduced by the drag free control system by a factor 50000 (Table 5 of the GG proposal). An inertial acceleration equal and opposite to it acts on each suspended mass inside the spacecraft, causing a displacement of its equilibrium position. The PGB on which are located the beam launchers of the laser gauge is displaced (with the test cylinders inside it) by 13 nm (using data of Table 5 and Table 6 in the proposal), while the test cylinders are displaced (in common mode) relative to it and in the same direction by 1 nm. As a result, the relative displacement between the PGB and the test cylinders amounts to 12 nm.

Such a common mode displacement of the test cylinders relative to the beam launchers is not a problem for the differential measurement to be performed.

b) Do the cited laser gauge demonstrations include the masking technique that would be used on GG?

The laser gauge realised by M. Shao for the SIM mission [21] has been implemented using exactly the same masking technique, as shown in Fig. 3. The noise level achieved is reported in Fig. 4. An arrangement of masks and mirrors suitable for GG has been studied.

c) There is no discussion of cross-talk between the two masked beams. How precisely does the wavefront need to be divided given that diffraction effects would cause cross-coupling between the two readouts?

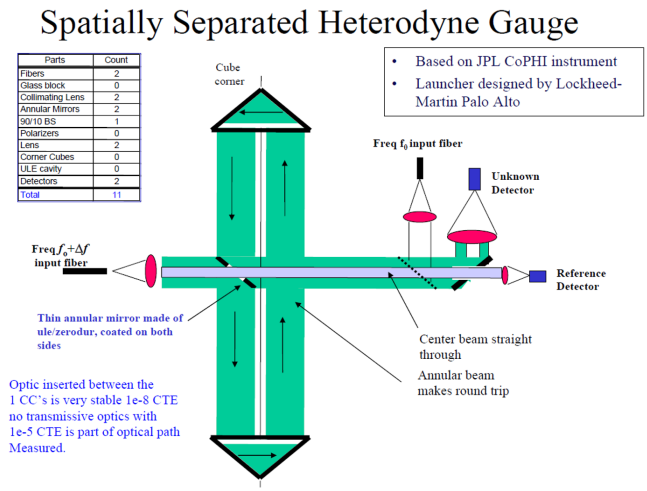

FIG. 3: Schematic of the interferometer used as a demonstrator of the spatial separation principle. The interferometer was developed for the SIM mission

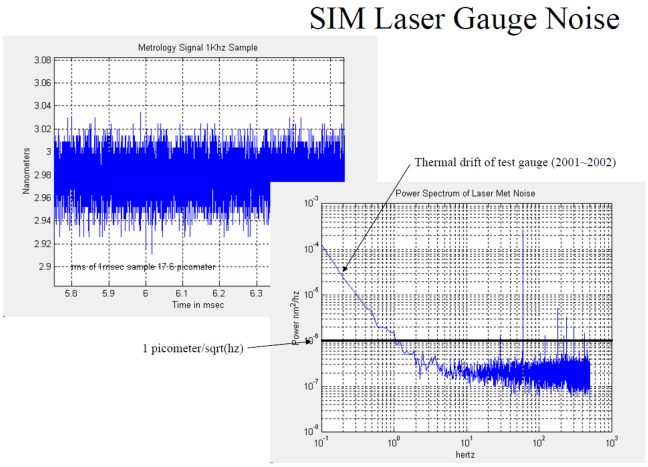

FIG. 4: Noise level of the SIM laser gauge outlined in the previous figure.

Diffraction caused by apertures and stops will cause cross-talk, hence nonlinearities. In fact this effect has been calculated for different set-ups and different scales, and can be reduced to the desired level.

Other possible causes of cross-talk could be present, such as spurious reflection on the surfaces of the corner cube retroreflectors and of the beam splitters. For this reason experimental results are usually worse than theo-

retical ones and the only reliable validation method is by experiment. In Fig. 5 owe show how diffraction can cause cross.talk.

In the SIM gauge non linearities at 10 pm level have been demonstrated. In GG smaller optics will be used and a larger diffraction effect is expected. The one year development mentioned in the proposal includes the evaluation of this effect and its minimization.

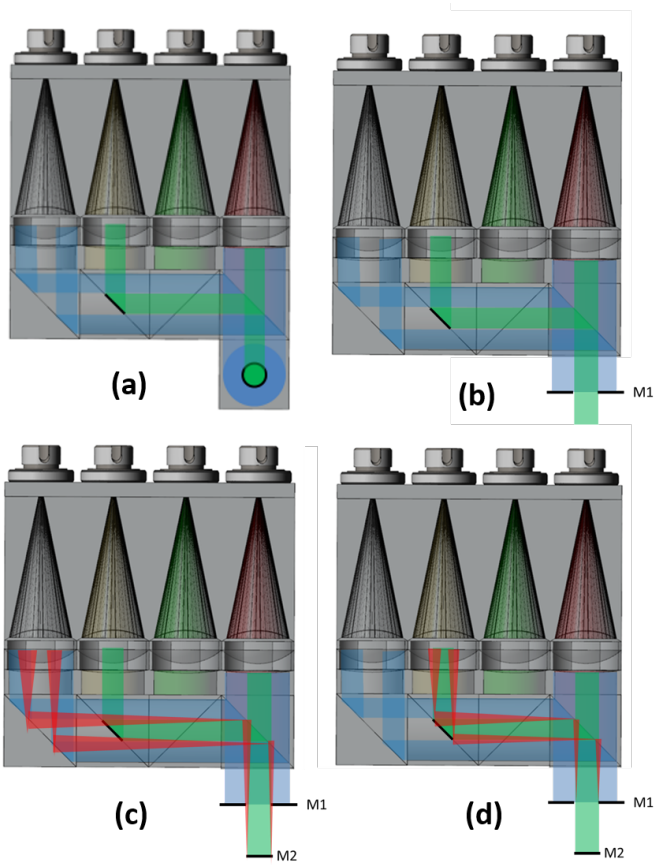

FIG. 5: Diffraction and cross-talk. a) Schematics of the laser gauge head. b) Same schematics with unfolded optical path for the sake of clarity. Mirrors M1 and M2 represent the reflectors mounted on the two masses. c) The effect of diffraction on the apertures causes some of the light reflected by M2 to mix with the light coming from M1 causing distortion. d) The complementary effect causing similar results.

The diffraction effect will be measured with a smaller set-up based on a compact assembly of beam splitters with 15 mm side and collimators with 15 mm diameter. If necessary, the effect will be minimized by using modulated reflectance masks in order to reduce diffraction and by shadowing part of the beams right in front of the collimators.

Finally, we point out that a nonlinearity level as low as 10 pm is not necessary for the GG laser gauge. In fact, since the differential displacement of the masses close to the measurement frequency is within 1 nm (see item e) below), which is less than 1/100 of the half period of the non-linearity, the residual error is less than 0.1 pm. Which means that in this specific application we have a safety margin of almost one order of magnitude.

d) Please describe the laser power requirements and the level to which power fluctuations can be tolerated to prevent the introduction of cylinder tilting.

The above noise represents a few microW of detected laser power. The detector noise is $< 1\text{pW}/\sqrt{\text{Hz}}$, hence a laser power of 1 μW gives a SNR of 10^6, hence $10^{-6}\,\lambda$ in 1 s, namely 1 pm in 1 s. The force due to radiation pressure is negligible (a few fN). Furthermore, though Nd:YAG lasers are already very stable, they can be power stabilized to minimize possible spurious effect that could affect the phase measurement.

e) How sensitive is the interferometer to beam alignment jitter induced by temperature fluctuations and relative motions of the two cylinders?

We have tried to model the effect of temperature changes on pointing stability. Based on our experience in building highly stable interferometric assemblies we have estimated a maximum drift at the measurement frequency of 1 μrad. The misalignment has two main effects: the first is a direct change of the optical path and the second is a change in the coupling efficiency in the detector fibers. The first one can be simply modelled as a classic cosine error and can be estimated as low as 0.02 pm at 1 Hz. The second effect implies a small change in intensity on the detector, which in turn could have a second order effect on the phase measurement. That is difficult to model and, although we expect it to be negligible, we will evaluate it during the development of the laser gauge.

As shown in Table 6 of the GG proposal, the requirement on the maximum relative displacement of the test cylinders is 1 nm, due to whirl motion at the natural differential frequency of $\frac{1}{540\,\text{s}} = 1.85 \cdot 10^{-3}$ Hz which in the rotating frame is up-converted close to the spin/measurement frequency by this amount.

V. The executive summary states "... confirmation would strongly constrain physical theories."

Q6. Could you give explicit examples of theories that would be constrained by a null result?

Following the statement "... confirmation would strongly constrain physical theories", the Executive Summary provided no references, neither they were given in Sec. 1.2 devoted to "The science case". This was a choice, since many theories predict a violation of the Weak Equivalence Principle and the Universality of Free fall (WEP/UFF) but there are no firm predictions as to the level at which a violation should occur, and if a prediction is made, it often depend on a number of poorly known parameters.

The key argument, in our view, is that once the test is improved by 4 (hopefully 5) orders of magnitude beyond the current limit, and WEP still holds, then any theory will have to come to terms with this fact. More importantly, if WEP is not violated at such deep levels, maybe "it is the truth" and one should think at something completely new. After the Michelson and Morley null result, people had to come to terms with the fact that the ether did not exist, and moved along a new root.

Nonetheless, we are obviously very interested in all theories that predict WEP/UFF violation.

Modifications to General Relativity (GR) are strongly motivated by the desire to make it compatible with quantum theory (Quantum Gravity) and with the observed and as yet satisfactorily unexplained astrophysical and cosmological features like flat rotation curves of galactic components ("dark matter" within GR and standard gravity), late acceleration of the expansion of the universe ("dark energy" or cosmological constant within standard GR).

Essentially all suggested modifications, especially those motivated by the most widely studied candidate quantum gravity theory –string theories– predict new fields (like dilaton, modulii) with coupling matter that depends on composition and hence violate WEP/UFF and universality of free fall (UFF) [22, 23]. This general expectation is expressed by Damour as "We emphasize the unsatisfactory fact that the EP maintains the absolute character of the coupling constants of physics, while general relativity and its generalizations (Kaluza–Klein,..., string theory) suggest that all absolute structures should be replaced by dynamical entities." Specific examples for several theories that will be constrained by a null UFF result are reviewed in [23].

Though not known with certainty, but estimates of such equivalence principle violations range from 10^{-13} to 10^{-18} (see e.g. [23, 24].)

Therefore, a null result at the level of 10^{-17}, and only at this level, will eliminate a major and highly significant portion of the parameter space available. This should be seen in the context that almost no other experimental clue is available to constrain string theory phenomenology today and WEP violation is a generic and nature feature in such theories.

Fig. 1 in [25] is indicative of a general scenario, where the relative differential acceleration is plotted against parameters of a string-inspired phenomenological theory. (The actual details also depend on the range of the interaction of new hypothetical fields and GG and other space experiments probe long range fields of scale size larger than the earth radius.)

Searches for Lorentz and CPT violation are a complementary approach to searching for clues regarding physics at the Planck scale. The gravitational Standard-Model Extension (SME) provides a general theoretical framework for such searches. Certain types of Lorentz violation in the SME are observable only in gravitational experiments [26], and space-based WEP tests such as GG are the most sensitive proposed experiments for probing these effects [27]. Moreover, such signals involve a characteristic time dependence making them distinguishable from other sources of WEP violation. The GG experiment would extend the maximum experimental sensitivity to this class of Lorentz-violating effects by at least 4 orders of magnitude and sensitivity to certain poorly constrained possibilities could be extended by up to 11 orders of magnitude. Hence a null result would significantly constrain the parameter space. While the SME is a general test framework, it contains many specific models that would be constrained by the GG experiment. These include the following. (1) Isotropic WEP Models, in which a special frame exists where effective WEP violation is the only leading order evidence of Lorentz violation. (2) Isotropic Invisible Models, in which the canceling of a CPT even coefficient against a CPT odd coefficient makes WEP violation invisible in a special frame, but observable in others. (3) Spacial Models, in which anisotropic WEP violation arises in all frames.

There are other scenarios that the null result will constrain effectively. One important set is theories that predict or accommodate time and space varying fundamental constants, especially the coupling constants for various fundamental interactions [28]. This affects the energy content of the mass elements used in the WEP experiment and leads to a violation of UFF [23]. While direct limits from atomic physics experiments are stringent, they are mostly limited to the fine structure constant, whereas a WEP experiment like GG is sensitive to all couplings. Hence, it is also sensitive to theories that explore the gravity sector of standard model extensions and Lorentz violations [26], albeit indirectly. Again, there are no firm predictions and theories will be constrained by GG a few orders of magnitude better than any previous WEP experiment.

The scenario of 'Chameleon' scalar field ("where a scalar field acquires a mass which depends on the local matter density: the field is massive on Earth, where the density is high, but is essentially free in the solar system"), introduced in the context of accelerated expansion of the universe, also has a natural violation of the WEP

and UFF, $\eta \sim 10^{-11}\beta^2 - 10^{-19}\beta^2$, where β is the parameter of the theory in its effective potential, of order unity and matter dependent [29]. (We note in passing that this theory also predicts a different value for G in solar system, compared to the lab measurements). Terrestrial tests are not effective in constraining because of a built in shielding mechanism and space experiments are essential. GG is the most effective experiment in design and validation that can constrain this scenario today.

Another important reason to improve tests of WEP is because it is fundamental for tests of the *Strong* equivalence principle (SEP), where UFF is tested for self-gravitating bodies. Very few alternative theories of Gravity predict SEP, general relativity being one of them. Current experimental constraints on SEP violation derived from limits on the Nordtvedt parameter from Lunar Laser Ranging (LLR) are already limited by the lack of precision of the WEP limits [30]. Despite the difficulties of LLR tests [31] strong efforts are ongoing in order to improve them and they will need better WEP tests than the current ones.

Surprisingly enough, there is also a rigorous prediction of WEP violation at the 10^{-17}, due to the work of Fischbach and collaborators [32]. They managed to calculate the contribution to the energy of a nucleus due to neutrino-antineutrino interaction, showing that a WEP test to 10^{-17} would constrain the coupling of gravity to neutrinos and to higher-order weak interactions.

VI. About the ground -based GGG experiment The executive summary states "... confirmation would strongly contain physical theories."

Q7. What progress has been made regarding the sensitivity of this experiment since the 2012 publication?

As a prototype of the GG experiment in space, the GGG laboratory prototype aims at achieving the best possible sensitivity to differential acceleration between the test cylinders at the frequency $\nu_{orb} \simeq 1.7 \cdot 10^{-4}$ Hz, which is the orbital frequency of GG and also the frequency of the target violation signal.

In 2012 GGG measured $\Delta a_{GGG2012} \simeq 7 \cdot 10^{-11}\,\mathrm{m/s^2}$ (see Ref. [33], Fig. 7).

In the GG M4 proposal Sec. 3.4 and Table 13 we reported having reached in 2014 $\Delta a_{GGG2014} \simeq 4.76 \cdot 10^{-12}\,\mathrm{m/s^2}$, with an improvement by a factor 15.7.

The result had been presented at the Microscope Colloquium III in Paris, November 2014 ([34], *Data analysis of equivalence principle test in space. Advantage of measurements in 2D and sensitivity of the laboratory prototype*) but was still unpublished. The page limit did not allow us to provide the necessary documentation in the proposal.

In addition to this result, in 2014 the GGG experiment allowed us to prove, for the first time, a very important theoretical prediction of rotordynamics concerning whirl damping that is worth reporting here because of its relevance.

An important consequence of the fact that the GG test cylinders are coupled in 2D and spin around the symmetry axis is that a similar rotating differential accelerometer can be realised at 1-g by using the vertical direction to suspend the cylinders against local gravity, by coupling them in the horizontal plane and by using a motor with bearings to spin.

The main role of the GGG lab prototype (full scale and with two degrees of freedom like the accelerometer to fly in GG) is to establish the sensitivity to differential accelerations that it can achieve at the frequency $\nu_{orb} \simeq 1.7 \cdot 10^{-4}$ Hz. It must be taken into account that: a) the test cylinders on ground (10 kg each as in GG) cannot be coupled as weakly as in absence of weight, which means a sensitivity scaling as the ratio of the respective differential periods squared (the relative displacement of the test masses produced by a differential acceleration is inversely proportional to their natural differential period squared); b) rotation noise (due to the motor and bearings) must be expected on ground though absent in space, and a weak rotating 2D joint has been implemented in order to reduce low frequency terrain tilt noise in the lab (also absent in space).

The GGG capacitance bridges provide the relative displacements of the test cylinders along the two orthogonal rotating directions of the sensitive plane a, b (as sketched in Fig. 1). After the 2012 publication [33] an improved version of the rotating readout electronics has been implemented and a new set of matched ball bearings has been mounted. In addition, a new data analysis strategy has been developed, based on complex Fourier analysis, which exploits in full the availability of output data along both axes of the sensitive plane (with the same level of electronic noise) and has considerable advantages [34].

The main idea is that output data in 2D make it possible to exploit the knowledge of the sign of spin in order to separate various error sources, in particular rotation noise (due to bearings and motor), which we know for sure that are absent in GG. This turns out to be much more advantageous than using the two channels to simply double the amount of output data.

In essence, the reasoning is as follows. Let us consider the rotating plane of sensitivity of the accelerometer, centered on one test mass (TM1), as a complex plane. The capacitance bridges give the position of TM2, namely its displacement relative to TM1, and we can combine the a, b coordinates to form the complex variable ζ (in point of fact it is a time series, the GGG readout yielding 32 data points per turn):

$$\zeta = a + ib \tag{21}$$

A violation signal at the orbital frequency ν_{orb} (with the same sign as the spin and $\nu_{orb} \ll \nu_{spin}$) as it is sought for by GG would be read in the complex plane as:

$$\zeta_{WEP} = \varrho_{WEP} e^{i(-\omega_{spin}-\omega_{orb})t} \tag{22}$$

since it would be caused by an Earth-like mass orbiting around the test cylinders located in the lab, a body that of course does not exist –our goal is to measure the GGG level of differential acceleration noise which would compete with such a signal. Thus, we know for sure that the relevant frequency is $-\nu_{spin}$, while this effect should not be found close to the frequency line $+\nu_{spin}$.

Instead, a disturbance oscillating at frequency ν_{orb} along a given direction of the horizontal plane of the lab (not due to a source body orbiting around the test masses), once transformed to the rotating complex plane, reads (we do not consider phase differences for simplicity):

$$\zeta_{osc} = \frac{\rho_{osc}}{2}(e^{i(-\omega_{spin}-\omega_{orb})t} + e^{i(-\omega_{spin}+\omega_{orb})t}) \quad . \tag{23}$$

Like the signal, this disturbance is close to the frequency line $-\nu_{spin}$ and should not be detected at all near $+\nu_{spin}$, because the system spins counterclockwise and not clockwise. However, unlike the signal, it has two frequency lines on opposite sides of $-\nu_{spin}$ at the same distance ν_{orb} from it and with the same amplitude (half of the total), while the signal appears on one side of $-\nu_{spin}$ only, which side depending on the sign of the orbital motion. In our complex Fourier analysis we distinguish a negative FFT^-, which should show both (22) and (23), from a positive FFT^+ in which neither of the two should appear. Similarly, for the spectral density we have SD^- and SD^+.

Electronics noise will obviously appear in both cases, since it is not related to the sign of spin.

In GGG we apply on purpose a differential force along one fixed direction of the horizontal plane, typically at 1 mHz, which in the rotating complex plane has the form (23). It is used for calibration (the two lines must have the same amplitude). Most importantly, it allows us to quantify how "noisy" is the rotation. Ideally, for a perfect counterclockwise rotation no "leakage" of the two spectral lines (23) should occur from FFT^- to FFT^+: we should find them only in FFT^- (the same in the case of the spectral density).

In Figs. 6 and 7, we report the time series (in the non rotating plane) for a one week duration run at $\nu_{spin} = 0.16\,\mathrm{Hz}$, the test cylinders being coupled in the sensitive plane with a natural differential frequency $\nu_{dm} = 0.074\,\mathrm{Hz}$ ($P_{dm} = 13.5\,\mathrm{s}$). Figs. 8 and 9 show the spectral densities and FFTs (in the rotating frame) as obtained with the complex Fourier analysis briefly described above.

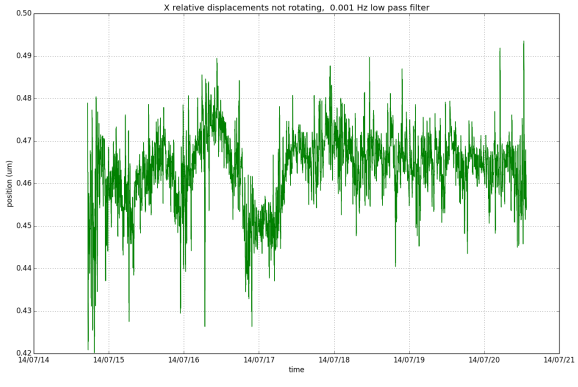

FIG. 6: Time series (for about one week of integration time) of the relative displacements of the test cylinders after demodulation to the (non rotating) horizontal plane of the lab: x axis. The centers of mass stay within $0.08\,\mu$m from each other. The spin frequency (counterclockwise) is $\nu_{spin} = 0.16\,\mathrm{Hz}$. The natural differential frequency is $\nu_{dm} = 0.074\,\mathrm{Hz}$ natural differential frequency ($P_{dm} = 13.5\,\mathrm{s}$).

Rotation noise "leakage" as discussed above is clearly visible in Figs. 8 and 9. Since it is due to bearings and/or motor, not present in GG, this is in fact a partial rejection (from the red to the blue curve) of rotation noise. We therefore use the blue curves to estimate (at the orbital frequency of GG indicated by the dashed lines) the level of noise relevant for GG. At this frequency we have:

- Lowest relative displacement noise (in $\mathrm{m}/\sqrt{\mathrm{Hz}}$): $\simeq 2 \cdot 10^{-8}\,\mathrm{m}/\sqrt{\mathrm{Hz}}$

- Lowest relative displacement noise (20 days): $\simeq 2.2 \cdot 10^{-11}\,\mathrm{m}$

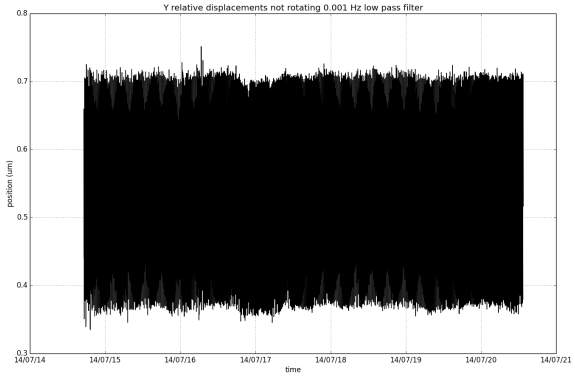

FIG. 7: Same time series as in Fig. 6 for the y axis of the lab. Along this direction the 1 mHz differential signal is applied and it is dominant.

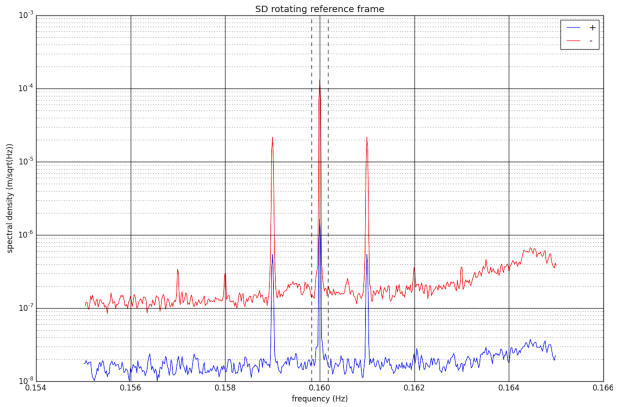

FIG. 8: Spectral Densitiy (SD) in the rotating frame as obtained with complex analysis, negative (SD^- red) and positive (SD^+ blue). The applied signal appears as expected with two lines on the opposite sides of $\nu_{spin} = 0.16\,\mathrm{Hz}$. Since the spin is counterclockwise, the two lines should appear only in the red curve. Instead, leakage to the blue one is apparent. Two vertical dashed lines are plotted at distance $\nu_{orb} = 1.7 \cdot 10^{-4}\,\mathrm{Hz}$ from the spin frequency, which is the frequency of a violation signal for GG in space, either on one or on the other side of the spin frequency. The feature to the right, on both the red and the blue curve, is probably due to an excess noise in some of the ceramic balls in the bearings (local lack of lubricant or tiny dust particles).

- Lowest differential acceleration noise, with 0.074 Hz differential frequency (in $\mathrm{ms}^{-2}\sqrt{\mathrm{Hz}}$):

  $\simeq 2 \cdot 10^{-8} \cdot (2\pi \cdot 0.074)^2\,\mathrm{ms}^{-2}/\sqrt{\mathrm{Hz}} \simeq 4.3 \cdot 10^{-9}\,\mathrm{ms}^{-2}/\sqrt{\mathrm{Hz}}$

- Lowest differential acceleration noise (20 days): $\simeq 4.76 \cdot 10^{-12}\,\mathrm{m/s}^2$

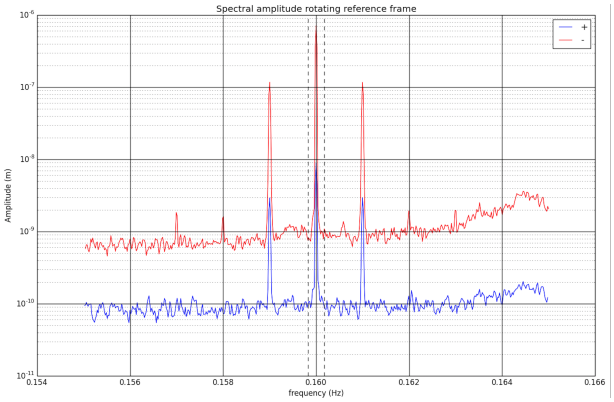

FIG. 9: FFT as derived from the spectral density of Fig. 8, in the rotating frame with complex analysis, negative (FFT^- red) and positive (FFT^+ blue). The sampling frequency is $\nu_{sampl} = 32\nu_{spin}$ and the resolution time is $T_{res} = 86400\,\mathrm{s}$. See also the caption of the previous figure.

We now compare the best sensitivity of GGG:

$$\Delta a_{GGGprototype1.7\cdot10^{-4}\,\mathrm{Hz}} \simeq 4.76\cdot10^{-12}\,\mathrm{m/s^2} \qquad (24)$$

with the differential acceleration that GG must measure (at the same frequency) to meet its baseline target $\eta = \frac{\Delta a}{g(h)} = 10^{-17}$:

$$\Delta a_{GGtarget} = 8.1\cdot10^{-17}\,\mathrm{m/s^2} \qquad (25)$$

showing that the GGG prototype is a factor $5.9\cdot10^4$ away from the GG target.

However, we recall that the coupling of the test masses is much stiffer on ground than in absence of weight, and the sensitivity scales as the ratio of the (respective) natural differential periods squared: $(\frac{540}{13.5})^2 = 1600$.

GG is designed for space, for the strong reasons presented in Sec. 1.4 of the proposal. The purpose of GGG is to validate the main features of GG, but its test masses cannot possibly be coupled as weakly as in absence of weight. On ground the most sensitive instrument is the torsion balance. With a natural (torsional) period of 790 s it is even more sensitive than GG in space, but it is not suitable for space. Thus, there is no way that the sensitivity gap by a factor 1600 between GG and GGG can be significantly reduced. This means that, at the current sensitivity reported here, GGG is only a factor $\frac{5900}{1600} = 37$ away from the best result it can provide as a prototype of GG. Trying to further reduce this factor is worthwhile only if GG will fly, to gain even better insights on its physical features. We note in passing that if GGG with the sensitivity (24) were to fly, it would provide a test of WEP to $5.9\cdot10^{-13}$.

In 2014 GGG has provided another important result concerning whirl damping.

It is well known in rotordynamics, and it has been shown also in response to Q3, that the forward whirl (which in a very low dissipation system like GG occurs at the natural frequency) grows exponentially depending on losses in the suspensions at the spin frequency, not at the natural frequency. Since the quality factor (inverse of the loss angle) is known to be higher at higher frequencies we should expect that when the system spins the whirl grows with a (negative) Q higher than the (positive) Q with which, at zero spin, an oscillation at the same natural frequency decays.

In 2014 when GGG was spinning at $\nu_{spin} = 0.16\,\mathrm{Hz}$ and the test cylinders whirled at a frequency of $\nu_w = 0.074\,\mathrm{Hz}$ (the same as their natural differential frequency), the whirl control was turned off and the growth in amplitude was measured (see Fig. 10, top plot) yielding $Q_w = 2310$. Once the rotation was stopped (vacuum chamber kept closed, data taking on, temperature controlled as before) it was observed from the real time Fourier analysis of the output data that oscillations at the differential frequency ($\nu_{dm} = \nu_w$) were by far dominant, all other frequencies showing much smaller amplitudes. This situation is quite unusual, and has allowed us to measure very neatly the decay of the oscillations at the differential frequency. The result is reported in Fig. 10, bottom plot, and yields $Q_n = 885$. As expected from theory, it is smaller than $Q_w = 2310$ measured in rotation. Though the ratio spin-to-natural frequency is quite low in GGG ($\frac{0.16}{0.074} = \frac{13.5}{6.25} = 2.16$) the effect on the quality factors is apparent: $\frac{2310}{885} = 2.61$, not far from the ratio in frequencies.

This measurement is important because most supercritical rotors used in a wide variety of applications have losses far much larger than GG, whirl is not finely damped and precise measurements such as these are rarely performed. With GGG we have confirmed experimentally a very relevant theoretical prediction of rotordynamics.

In GG a higher Q is expected for various reasons: a) the test cylinders spin at 1 Hz rather than 0.16 Hz (Q is higher at higher frequency); b) the relative displacements are much smaller than on ground (Q is higher at lower oscillation amplitude); c) the suspensions are tiny while on ground they must suspend 10 kg masses.

Q has been measured for a CuBe spring (manufactured from a single block) in horizontal oscillation at 5 Hz yielding Q values close to 19000 for oscillation amplitudes much larger than in GG (see [1])

The requirement for GG is $Q \simeq 20000$ at 1 Hz (see Table 4 in the proposal) and certainly within reach.

Even with the value 2310 measured by GGG, because of the 540 s differential period of the GG test masses, once the whirl radius has been damped it would take almost 11 days for it to increase by a factor 10.

On ground, with the same Q, the whirl amplitude of the GGG test masses grows much faster (see Fig. 10, top plot) because the whirl period is much smaller (only 13.5 s). This is why in GGG whirl control is on all the time during the measurement runs, which however has not prevented a good sensitivity from being achieved. Instead, in GG whirl control will be always off during the

science measurements (see Table 6 of the GG proposal).

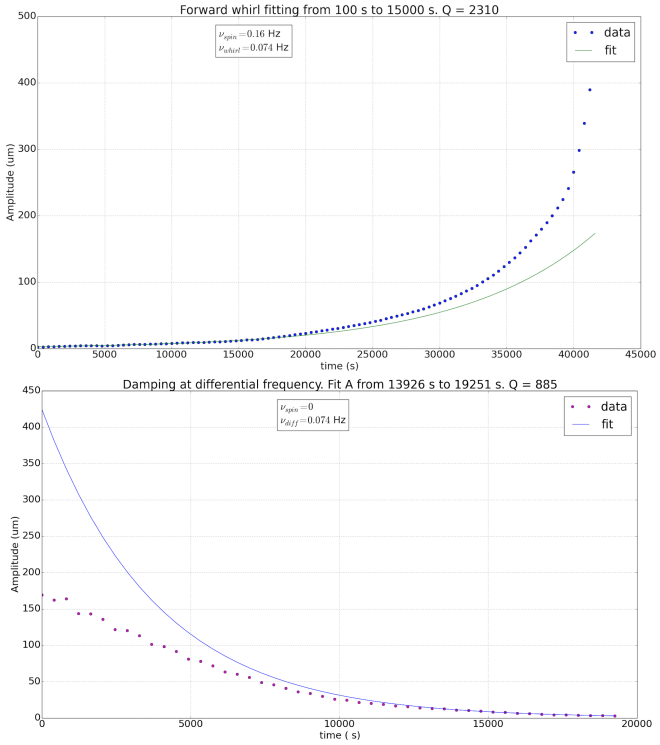

FIG. 10: Top: $Q = -2310$ as measured from the whirl growth at frequency $\nu_{whirl} = 0.074\,\text{Hz}$ while GGG is spinning at $\nu_{spin} = 0.16\,\text{Hz}$.
Bottom: $Q = +885$ as measured with GGG from the decay of the amplitude of oscillation at the natural differential frequency $\nu_{dm} = \nu_{whirl} = 0.074\,\text{Hz}$

[1] *"Galileo Galilei" (GG) Phase A Report*, ASI (Agenzia Spaziale Italiana), 1st edn. November 1998, 2nd edn. January 2000
http://eotvos.dm.unipi.it/ggweb/phaseA/

[2] P. Goldman & A. Muszynska, *Chaotic Behavior of Rotor/Stator Systems With Rubs*, J. Eng. Gas Turbines Power 116(3), 692-701 (1994)

[3] U. Ehehalt & R. Markert, *Instability of Unbalance Excited Synchronous Forward Whirl at Rotor-Stator-Contact*, Proc. App. math. Mecc. 2, 60-61 (2003)

[4] G. Adiletta, A. R. Guido & C. Rossi, *Chaotic motions of a rigid rotor in short journal bearings*, Nonlinear Dynamics 10, 251-269 (1996)

[5] R. Pegna *et al.*, Phys. Rev. Lett. 107, 200801 (2011)

[6] S. H. Crandall, J. Sound Vib. 11(1), 3-18, (1970)

[7] Y. Jafry & M. Weinberger M, Class. Quantum Grav. 15 481-500 (1998)

[8] A. M. Nobili et al., Class. Quantum Grav. 16, 1463-1470 (1999)

[9] *Review by S. H. Crandall on the stabilization of GG bodies* (1997)
http://eotvos.dm.unipi.it/eval/crandall/CrandallLett.jpg

[10] I. Ciufolini and J. A. Wheeler, *Gravitation and inertia* (Princeton University Press, Princeton, 1995)

[11] R. P. Kerr, Phys. Rev. Lett. 11, 237 (1963)

[12] N. Ashby and B. Shahid-Saless, Phys. Rev. D 42, 1118 (1990)

[13] W. de Sitter, Mon. Not. R. Astron. Soc. 77, 155 (1916)

[14] L. I. Schi, Physical Review Letters 4, 215 (1960

[15] J. Lense and H. Thirring, Phys. Z. 19, 156 (1918)

[16] C. W. F. Everitt, *et al.*, Phys. Rev. Lett 106, 221101 (2011)

[17] B. M. Barker & R. F. O'Connell, Phys. Rev. D 12, 329-335 (1975

[18] *"GG Preliminary Requirements Review Data Package (GG-PRR-Data-Pack)"*, ASI-Thales Alenia Space Contract No. I/039/08/0 "Studio di Fase A2 della Missione Galileo Galilei-GG", 2008-2009

[19] A.M. Nobili *et al.*, Phys. Rev. D 89, 042005 (2014)

[20] G. Vannaroni & R. Bruno, *Electrostatic Venting Device for the Pico Gravity Box of the GG spacecraft*, Note for the GG industrial study (2009)

[21] M. Shao "SIM: the space interferometry mission", Proc. SPIE 3350, Astronomical Interferometry, 536 (July 24, 1998); doi:10.1117/12.317092

[22] C. M. Will, Living Rev. Relativity 17, 4 (2014)

[23] T. Damour, Class. Quantum. Grav. 29, 1840001 (2012)

[24] J. Overduin *et al.*, Class. Quantum. Grav. 29, 184012 (2012))

[25] T. Damour and A. M. Polyakov, Nucle. Phys. B423, 532 (1994)

[26] V. A. Kostelecky and J. D. Tasson, Phys. Rev. Lett. 102, 010402 (2009)

[27] V. A. Kostelecky and J. D. Tasson, Phys. Rev. D 83, 016013 (2011)

[28] G. Dvali & M. Zaldarriaga, Phys. Rev. Lett. 88, 091303 (2002)

[29] J. Khoury and A. Weltman, Phys. Rev. Lett. 93, 171104 (2004)

[30] F. Hofmann, J. Müller, and L. Biskupek, Astronomy and Astrophysics, 522, L5 (2010)

[31] A. M. Nobili *et al.*, General Relativity & Gravitation 40, 1533-1554 (2008)

[32] E. Fischbach *et al.*, Phys. Rev. D 52, 5417-5427 (1995)

[33] A.M. Nobili *et al.*, Class. Quantum Grav. 29, 184011 (2012)

[34] A. M. Nobili & A. De Michele, *Data analysis of equivalence principle test in space. Advantage of measurements in 2D & sensitivity of the laboratory prototype*, talk given at Microscope Colloquium III, Onera, Paris (November 2014)